Author/s:
Zheng, F;Zuo, C;Niu, M;Zhou, C;Bradley, SJ;Hall, CR;Xu, W;Wen, X;Hao, X;Gao, M;Smith, TA;Ghiggino, KP

Title:
Revealing the Role of Methylammonium Chloride for Improving the Performance of 2D Perovskite Solar Cells

Date:
2020-06-10

Citation:
Zheng, F., Zuo, C., Niu, M., Zhou, C., Bradley, S. J., Hall, C. R., Xu, W., Wen, X., Hao, X., Gao, M., Smith, T. A. & Ghiggino, K. P. (2020). Revealing the Role of Methylammonium Chloride for Improving the Performance of 2D Perovskite Solar Cells. ACS Applied Materials and Interfaces, 12 (23), pp.25980-25990. https://doi.org/10.1021/acsami.0c05714.

ACS APPLIED MATERIALS & INTERFACES

Energy, Environmental, and Catalysis Applications

Revealing the Role of Methylammonium Chloride for Improving the Performance of 2D Perovskite Solar Cells

Fei Zheng, Chuantian Zuo, Mengsi Niu, Chunhua Zhou, Siobhan Bradley, Christopher Hall, Weilong Xu, Xiaoming Wen, XiaoTao Hao, Mei Gao, Trevor A. Smith, and Kenneth P. Ghiggino

ACS Appl. Mater. Interfaces, **Just Accepted Manuscript** • DOI: 10.1021/acsami.0c05714 • Publication Date (Web): 18 May 2020

Just Accepted

is published by the American Chemical Society. 1155 Sixteenth Street N.W., Washington, DC 20036

Revealing the Role of Methylammonium Chloride for Improving the Performance of 2D Perovskite Solar Cells

Fei Zheng,[1] Chuantian Zuo,[2] Mengsi Niu,[3] Chunhua Zhou,[4] Siobhan J. Bradley,[1] Christopher R. Hall,[1] Weilong Xu,[1] Xiaoming Wen,[4] Xiaotao Hao,[3,1] Mei Gao,[2,*] Trevor A. Smith,[1] Kenneth P. Ghiggino[1,*]

[1]*School of Chemistry and ARC Centre of Excellence in Exciton Science, The University of Melbourne, Parkville, Victoria 3010, Australia*

[2]*Flexible Electronics Laboratory, CSIRO Manufacturing, Clayton, Victoria 3168, Australia*

[3]*School of Physics, State Key Laboratory of Crystal Materials, Shandong University, Jinan 250100, Shandong, China*

[4]*Centre for Translational Atomaterials, Swinburne University of Technology, Hawthorn, Victoria 3122, Australia*

*Email: ghiggino@unimelb.edu.au; Mei.Gao@csiro.au

ABSTRACT:

Layered perovskite films, composed of 2D Ruddlesden-Popper perovskites (RPP), show improved stability compared to their conventional 3D counterparts in perovskite solar cells (PSCs). However, 2D PSCs exhibit a lower power conversion efficiency (PCE) that has been attributed to compositional inhomogeneity and non-uniform alignment of the 2D perovskite phases. Methylammonium chloride (MACl) has been adopted as an additive to improve the PCE and the operational stability of 2D PSCs, although the role of MACl in performance enhancement is unclear. In this work, time and spatially-resolved fluorescence and absorption techniques have been applied to study the composition and charge carrier dynamics in MACl doped $BA_2MA_4Pb_5I_{16}$ ($<n>=5$) layered perovskite films. The inhomogeneous phase orientation distribution in the direction orthogonal to the substrate for undoped layered perovskite films undergoes reorganization upon MACl doping. Based on structural and crystallographic analyses, it is revealed that MACl can facilitate the crystallization of small-*n* 2D perovskite phases at the cost of consuming an increased amount of BA cations. Consequently, an increase in the thickness of large-*n* 2D perovskite phases accompanies their enhanced perpendicular alignment ([101] crystalline orientation) to the substrate, which facilitates charge carrier transport and collection by electrodes. The defect passivation of the MACl doped layered perovskite film provided by the small-*n* phase is also beneficial to the photovoltaic performance of the PSC device. A maximum PCE (~14.3%) was achieved at 6 mol% MACl doping, with this optimum level influenced by the increased interfacial roughness of the layered perovskite film caused by the edges of small-*n* perovskite flakes emerging on the front surface.

KEYWORDS: 2D, layered perovskite film, MACl doping, small-*n*, large-*n*, perpendicular

INTRODUCTION

Two-dimensional (2D) Ruddlesden-Popper perovskites (RPP), denoted by the formula of $R_2A_{n-1}Pb_nX_{3n+1}$, are steadily gaining interest in both fundamental theoretical and experimental investigations owing to their unique optical properties and the potential for optoelectronic applications.[1-4] The structure of 2D perovskites is generally described as *n* layers of 2D $[PbX_4]^{2-}$ octahedra sandwiched by two layers of long-chain alkylammonium cations (or ligands) (R^+).[5] These 2D perovskites are essentially quantum wells (QWs) with a tunable band-gap depending on well width (layer thickness, *n*) in which the electrical insulating long-chain cations act as barriers and provide quantum and dielectric confinement to electrons.[6] Significantly, the hydrophobic alkylammonium ligands (R^+) can prevent moisture invasion into perovskite crystals, imparting 2D perovskites with improved humidity and atmosphere resistance compared to their 3D counterparts.[1] Despite the insulating nature of the long-chain cation layers, the alignment of the 2D perovskite flakes perpendicular to the substrate ensures considerably high carrier mobility of the films in the direction orthogonal to the substrate.[7] Therefore, as has been widely reported,[1, 5, 8] perovskite solar cells (PSCs) based on 2D layered perovskite films show superior environmental stability while maintaining high power conversion efficiencies (PCEs).

Phase pure 2D perovskite crystals with the desired *n* value can be synthesized by supersaturation methods from the precursor solution with a controlled R to A ratio (2: n-1) according to the given molecular formula.[9] Alongside the structural analysis of 2D perovskite crystals by X-ray crystallographic diffraction, physical properties such as the exciton binding energy and polaron dynamics in small-*n* 2D perovskite phase are also intensively studied to provide a clearer picture of these materials.[4, 10] Layered perovskite films, cast from 2D perovskite precursors (with specific *n* value), required for PSC applications, are not composed of a single component of *n*-layer 2D perovskite but rather a mixture of 2D perovskites with various thicknesses.[7] This phenomenon can be easily verified by the different photoluminescence (PL) emission observed between the front and back (film-substrate interface) surface of layered perovskite films. Therefore, the phase distribution and orientation profiles of 2D perovskite layers within the layered perovskite film become critical issues influencing the charge carrier dynamics and thus the performance of PSCs. Unfortunately, a clear understanding of the structure of layered perovskite films is still lacking. Chen et al. determined that perpendicularly aligned (relative to the substrate) 2D perovskite flakes nucleate and grow from the top surface (liquid-air interface) toward the bottom (substrate) side during the formation of layered perovskite films.[11] In contrast, recent work by Huang's group revealed that 2D components are concentrated at the bottom of deposited films and 3D-like phases are present on the front surface.[12]

To achieve ordered alignment and homogeneous phase distribution of 2D perovskite flakes, critical for the performance of 2D PSCs, investigations based on synthetic control,[13] solvent engineering,[14, 15] and additives doping of layered perovskite films have been carried out.[16] Among these, doping holds the advantage of easy processability and excellent reproducibility. Inspired by the application of chloride in achieving high-quality 3D $MAPbI_{3-x}Cl_x$ perovskites,[17] small amounts of methylammonium chloride (MACl) were doped into the precursor of the 2D perovskite for the deposition of layered perovskite films, yielding improved photovoltaic performance of PSC devices. The power conversion efficiency (PCE) of PSCs based on 2D perovskite $(ThMA)_2(MA)_{n-1}Pb_nI_{3n+1}$ ($<n>$ = 3) was dramatically improved from 1.74% to 15.42% using MACl as the additive as reported by Lai et al.[16] The use of DMSO solvent and 10 mol% MACl additive was found to provide a synergistic effect to achieve a hysteresis-free PSC based on $(PEA)_2(MA)_3Pb_4I_{13}$ ($<n>$=4) RPP, with a PCE exceeding 12%.[18] Although the performance enhancement of devices upon MACl doping is correlated to the morphology and crystallinity improvement of layered perovskite films, the role of chloride ions in tailoring the film structure remains controversial. For example, Chen et al. proposed that chloride ions are incorporated to form the $PbCl_6^{4-}$ based 2D perovskite phase forms in the chloride doped layered perovskite films.[19] Recently, other research has demonstrated that chloride ions only exist in the intermediate phase and are finally eliminated during the MACl additive assisted preparation of pure α-phase formamidinium lead iodide ($FAPbI_3$)-based perovskite.[20] A clear understanding of film structure and the formation mechanism of layered perovskite films is urgently needed for the further improvement of 2D PSC devices upon MACl additive doping or by other methods.

In this work, we demonstrate effective PCE enhancement and reduced hysteresis for PSC devices based on 2D $BA_2MA_4Pb_5I_{16}$ ($<n>$=5) layered perovskite film upon MACl doping. To uncover the role of MACl and the mechanism driving the performance improvement, systematic characterizations were carried out on the layered perovskite films without and with MACl additives. Spatially resolved photoluminescence (PL) measurements show that the thickness of the large-*n* 2D perovskite phase, which dominates the composition of layered perovskite films, increases with an increasing MACl doping ratio. The enhanced alignment preference of large-*n* 2D perovskite flakes as indicated by powder XRD is achieved upon MACl doping, which is favorable for efficient charge transport in the direction orthogonal to the substrate. Time-resolved PL and transient absorption techniques compare the charge carrier dynamics in layered perovskite films without and with MACl doping, further supporting the efficient charge carrier funneling from small-*n* to large-*n* 2D components inside the film with the fastest electron transfer at the perovskite/ETL interface for the film with 6 mol% MACl doping. Finally, we propose that MACl can facilitate the crystallization of small-*n* 2D perovskite flakes, leading to a thickness increase and thus a more enhanced alignment profile of the large-*n* 2D perovskite component in the MACl doped layered perovskite films. Together with the decreased trap state density offered by the passivation effect of the small-*n* 2D component, the PCE of PSC

devices was thus considerably increased from 8.2±0.3% to 13.9±0.3% with 6 mol% being the optimal MACl doping.

RESULTS AND DISCUSSION

To clarify the composition and structure of layered perovskite films more confidently, the photoluminescence properties of 2D perovskite crystals with various thicknesses (represented by the number of $[PbX_4]^{2-}$ octahedral layers: *n*) were first studied. **Figure 1a** shows the normalized PL spectra of 2D $BA_2MA_{n-1}Pb_nI_{3n+1}$ (*n*=1, 2, 3, 4, 5) and 3D $MAPbI_3$ (*n*=∞) perovskite crystals (with photographs shown in **Figure S1a,** Supporting Information) excited by a 400 nm femtosecond pulsed laser. Except for the PL spectrum of the 2D *n*=5 perovskite, all spectra feature a narrow peak, indicating the high purity of these synthesized perovskite crystals.[21] A small amount of PL emission from the *n*=4 phase can be recognized from the spectrum of the *n*=5 perovskite crystal sample, which is in keeping with the consensus that it is difficult to synthesize phase-pure 2D perovskites with large layer thicknesses. The structures of 3D $MAPbI_3$ and 2D $BA_2MA_{n-1}Pb_nI_{3n+1}$ (*n*=1, 2, 3) are schematically illustrated in the inset of **Figure 1b**. For 2D perovskites, PL emission is generated by the radiative recombination of excitons. The PL peak position (λ_{PL}) is determined by the excitonic gap (E_x), or optical gap,[22] through Equation 1:

$$E_x = E_g - E_b = \frac{h \cdot c}{e \cdot \lambda_{PL}} \quad (1)$$

where h is Planck's constant, c is the velocity of light in vacuum, e is the conversion from Joules to eV (1 eV=1.6 × 10^{-19} Joules), and E_g, E_b are the energy bandgap and exciton binding energy, respectively. The observed redshift of the PL peak with the gradual increase of the *n* value is consistent with literature reports, and can be correlated to the reduced quantum confinement induced by spacer cations with the thickness increase of the inorganic slabs. As shown in **Figure 1b**, the variation of E_x for 2D and 3D perovskite crystals as a function of *n* can be well fit by Equation 2.

$$E_x = 1.623\ eV + \frac{1\ eV}{0.063 \cdot n^2 + 0.458 \cdot n + 0.811} \quad (2)$$

In this equation, 1.623 eV is the E_x of 3D $MAPbI_3$ perovskite, which can also be regarded as the bandgap (E_g) due to the small E_b value reported for 3D perovskite. Based on this equation, the *n* value of specific 2D $BA_2MA_{n-1}Pb_nI_{3n+1}$ perovskite can be easily determined using the PL peak position.

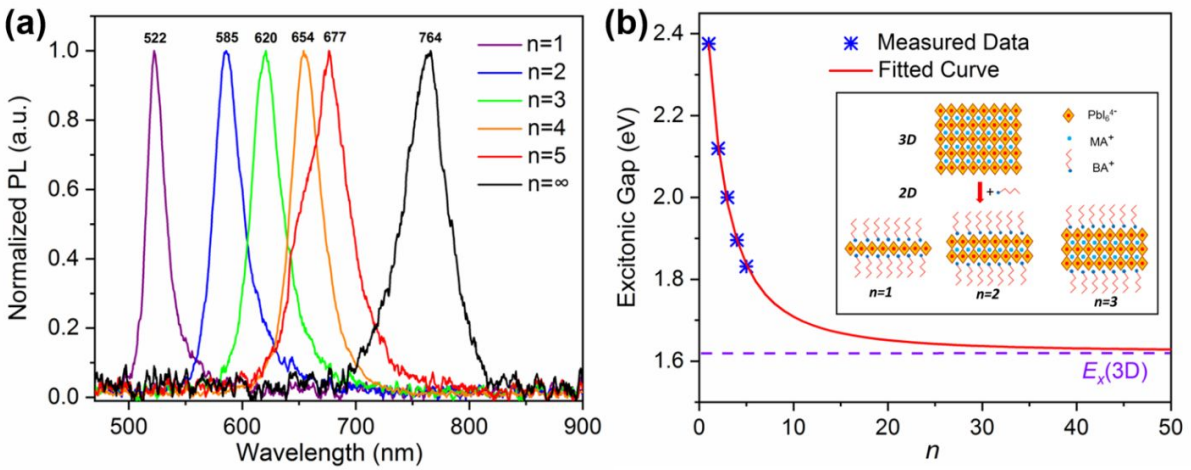

Figure 1. (**a**) Normalized PL spectra of 2D $BA_2MA_{n-1}Pb_nI_{3n+1}$ (n=1, 2, 3, 4, 5) and 3D $MAPbI_3$ (n=∞) perovskite crystals; (**b**) Plot of the excitonic gap of 2D perovskite crystals with n value and the corresponding fitted curve using Equation 2. (Inset: schematic illustrations of the structure of 2D and 3D perovskites).

PSCs based on nominally <n>=5 layered perovskite films with 0 mol% (non-doped, with appearance shown in **Figure S1b**), 3 mol%, 6 mol%, 9 mol%, 12 mol% MACl doping, fabricated by the one-step drop-casting method,[23] were tested under standard AM1.5G illumination. Performance parameters including the short circuit current (J_{SC}), open circuit voltage (V_{OC}), fill factor (FF), and power conversion efficiency (PCE) of all devices obtained by the reverse scan are plotted in **Figure 2a**. With the gradual increase of MACl doping ratio from 0 mol% to 12 mol%, the PCE, J_{SC}, V_{OC}, and FF of the 2D PSC devices all increase first and then decrease. The maximum PCE value is achieved for the 6 mol% MACl device (13.9±0.3%), which is significantly improved compared to the 0 mol% MACl device (8.2±0.3%). As shown in **Figure S2**, the PCE of champion devices (14.3%) can retain ~98% of the initial value when stored in an N_2-filled glovebox for 100 days without encapsulation, implying the superior performance stability of 6 mol% MACl doped 2D PSCs. **Figure 2b** presents the J-V curves of champion devices based on 0 mol% and 6 mol% MACl doped layered perovskite films for comparison. An obvious J-V hysteresis can be observed in the 0 mol% MACl device, with a hysteresis factor (HF) of 10.61% defined as follows:[24]

$$HF = \left|\frac{FF_{Forward} - FF_{Reverse}}{FF_{Reverse}}\right| \times 100\% \quad (3)$$

In comparison, the hysteresis factor of the 6 mol% MACl device (2.99%) is rather small, confirming the reduced hysteresis characteristic of 2D PSCs with optimized MACl doping. The normalized maximum power output (MPP) curves of un-doped (0 mol% MACl) and optimized (6 mol% MACl) devices are shown in **Figure 2c**. For the non-doped device, a slow increase of the MPP appears after a rapid response to light illumination. The 6 mol% MACl device demonstrates a faster photo-response as the MPP almost reaches

the maximum value at the initial stage of light illumination. According to our previous report, this slow response of the MPP to light illumination results from the synergistic effect of the light-induced curing of defect sites and the accumulation of mobile ions at perovskite interfaces.[25] This suggests that MACl doping reduces the defect density and suppresses ion migration in layered perovskite films.[26] Further investigations were performed to investigate the underlying reasons for this observed relationship between the PCE of the 2D PSC device and the doping ratio of the MACl additive, to explore the role of MACl in the performance enhancement.

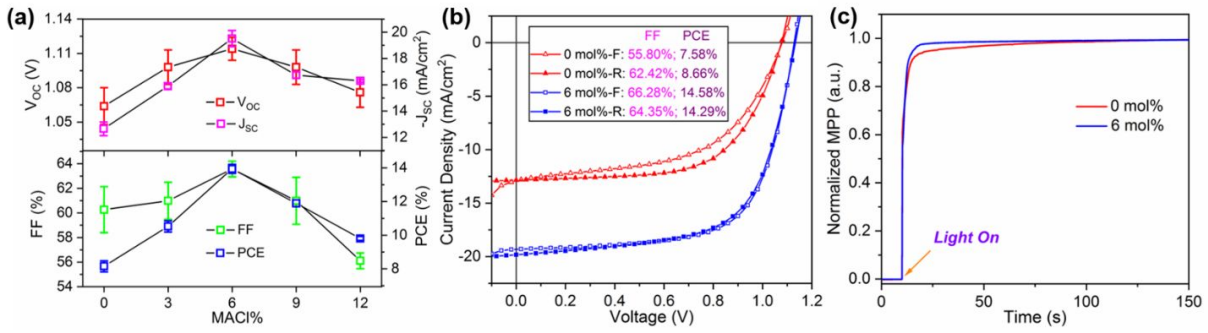

Figure 2. (**a**) V_{OC}, $-J_{SC}$, FF, and PCE of the 2D PSC device (obtained from reverse scan) plotted as a function of MACl doping ratio; (**b**) J-V curves of champion 0 mol% MACl and 6 mol% MACl PSC devices under both forward and reverse scans; (**c**) Normalized maximum power output (MPP) curves of 0 mol%, 6 mol% MACl PSC devices.

Steady state photoluminescence (PL) spectra of all these layered perovskite films were collected from both sides of the films in the reflection mode with a large excitation beam size (diameter ~100 μm). The penetration depth of the 400 nm excitation beam into the layered perovskite films is estimated to be ~100 nm based on the absorption spectra in **Figure S3**, indicating the fluorescence signals collected are mainly from the same side of the film as the photoexcitation. As shown in **Figure 3a**, PL spectra with illumination of the back side (film-substrate interface) of all films are composed of multiple peaks, including the relatively low intensity, peaks at short wavelengths and the dominant long wavelength PL peak. According to the data presented in Figure 1a and literature reports,[7] the short wavelength PL peaks seen in **Figure 3a** can be assigned to emission from n=2, 3, 4, 5 2D perovskite components, and the dominant peak at long wavelength is due to the 3D-like perovskite phase. Thus, the back side of the $\langle n \rangle$=5 layered perovskite film is composed of a phase mixture of various thickness 2D perovskite flakes and a 3D-like perovskite phase. In contrast, the PL spectra obtained from the front side (film-air interface) (**Figure 3b**) feature mainly the long wavelength peak from the 3D-like perovskite phase, which is consistent with literature reports.[12, 27] With the increase of the MACl doping ratio from 0 mol% to 9 mol%, PL peaks corresponding to both 2D perovskite flakes and the 3D-like component show significant intensity enhancement for both sides of the films. These can be attributed to the increased crystallinity of all perovskite phases and the decreased

density of defect states, which act as the quenching sites for charge carriers,[28] in the layered perovskite films upon MACl doping. As shown in the zoomed-in inset in **Figure 3b**, the PL peaks at short wavelength gradually increase with the higher level of MACl doping, indicating the appearance of small-*n* 2D perovskite flakes in the front surface of layered perovskite film. When normalized to unity (**Figure 3c, d**), an obvious redshift of peak position corresponding to the 3D-like perovskite phase, from 748 nm to 760 nm, with the increase of MACl doping ratio, can be seen for both sides of the film, while the peak positions of all small-*n* 2D perovskites remain constant. For each sample, the PL peak position of the 3D-like phase obtained from both sides of the film is similar with the increase of MACl doping. The peak positions of 3D-like phases for all samples are at relatively shorter wavelengths than that of real 3D perovskite (764 nm) presented in **Figure 1a**. Thus, we propose the existence of large-*n* 2D perovskite flakes, which have been previously recognized as 3D-like perovskite, that penetrate throughout the layered perovskite film for all samples. Based on Equation 2, the layer thickness (labeled as *n*=L) of large-*n* 2D perovskite from various MACl doped layered perovskite films is calculated and plotted in **Figure 3e**. A gradual thickness increase of the large-*n* 2D perovskite component in the layered perovskite film, from *n*=18 to 42, with the increase of MACl doping ratio can thus be revealed by these PL studies.

In addition, no PL emission from a $PbCl_6^{4-}$ based perovskite phase (2D or 3D), which would appear as a blue-shifted peak owing to the larger energy bandgap (E_g),[29, 30] was observed for any of the MACl doped layered perovskite films studied. The energy dispersive X-ray (EDX) analysis of the compositions of the 0 mol% and 6 mol% MACl perovskite films (**Figure S4**) provides further evidence for the absence of chlorine in the MACl doped sample. Hence we believe that chloride anions are expelled during the annealing process in the form of MACl molecules, similar to the situation studied in the 3D $FAPbI_3$ case.[20, 31]

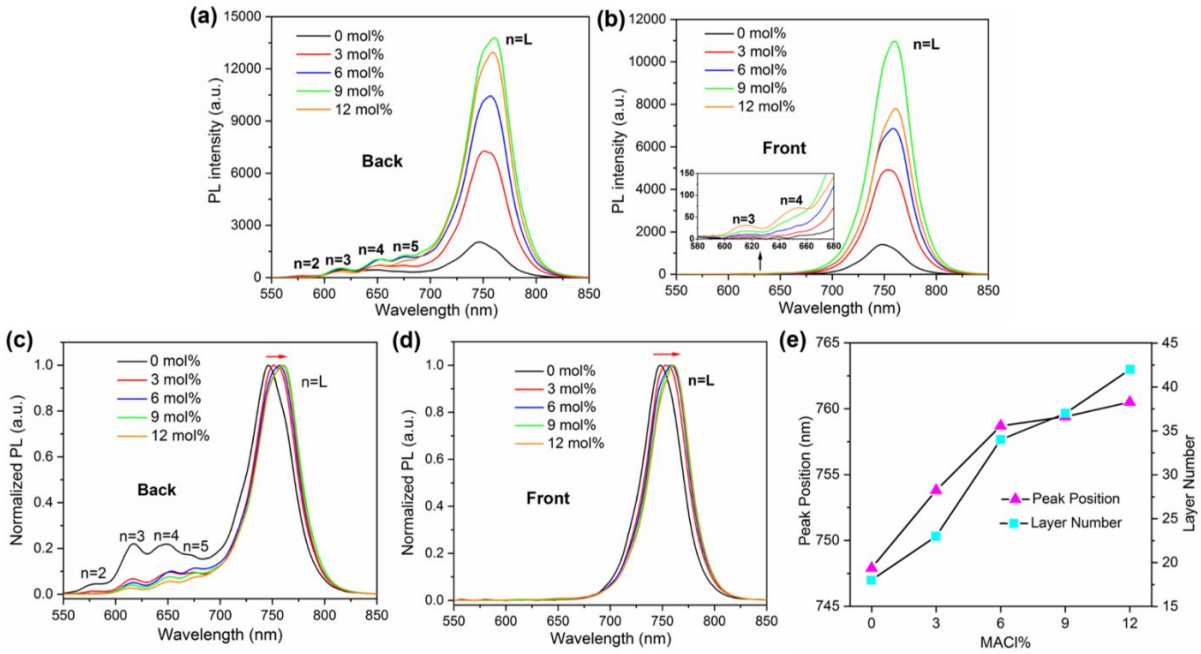

Figure 3. (**a, b**) PL spectra of layered perovskite films measured from the back (**a**) and front (**b**) surfaces; (Inset shows the zoomed-in spectra). (**c, d**) Normalized PL spectra of layered perovskite films measured from the back (**c**) and front (**d**) surfaces. (**e**) Plots of PL peak position (*n*=L) and calculated layer thickness (*n*) with MACl doping ratio (λ_{ex} = 405 nm)

To evaluate the morphology of layered films, optical microscopic characterization of the front and back surfaces of all layered perovskite films was carried out (**Figure S5**). From the optical images of the front surface (**Figure S5a-e**), an increased inhomogeneity in optical contrast can be observed for layered perovskite films with increasing doping ratio of MACl, showing more darkly-colored domains. Darker-colored aggregations of tens of micrometers in size are formed in the front surface of the layered perovskite film when the MACl doping ratio reaches 12 mol%. Considering the different optical properties of small-*n* and large-*n* 2D perovskite phases, and that the 0 mol% MACl film front surface is composed of only the lighter-colored regions, we assign the lighter-color regions to large-*n* perovskite and the darker-colored regions to the small-*n* perovskite phase (as labeled in **Figure S5g**). This color contrast is more obviously demonstrated in the optical images of the back surface as shown in **Figure S5f-j**. The dominant darker-colored regions present in the back surface of the 0 mol% MACl film and the gradual increase of the proportion of the lighter-colored regions in the back surface of films with increased MACl doping ratio is consistent with the observed relative intensity enhancement of PL emission from large-*n* perovskite revealed in **Figure 3c**.

Spatially resolved PL measurements were applied to further identify the composition of the aggregation domains formed in the 12 mol% MACl doped film sample. **Figure 4a** shows the optical image (20μm ×

20μm) of the front surface with aggregation domains (dark stripe) located in the image center. PL mapping of the same region (**Figure 4b**) exhibits the 2D spatial distribution profile of PL peak positions, revealing the concentration of short wavelength PL emission in the aggregation region. PL spectra (**Figure 4c**) of three selected points labeled in **Figure 4b** clarify the compositional difference between different regions of the film surface. A considerable amount of small-*n* (*n*=2, 3, 4, 5) 2D perovskite together with large-*n* 2D components can be found in the aggregation domain, while only large-*n* 2D perovskites are found outside the aggregation feature. The large-*n* (n~16-19) perovskite flakes in the aggregation region are also much thinner than in the lighter-colored region (*n*=43). This result further supports the assignment of the darker-colored region observed in the optical microscopy image to small-*n* phases and shows that increasing the doping of MACl in layered perovskite films causes the appearance of small-*n* perovskite components (darker-colored) in the front surface of the film. An excess amount of MACl doping can even lead to phase segregation of small-*n* 2D perovskite phases to form aggregation domains.

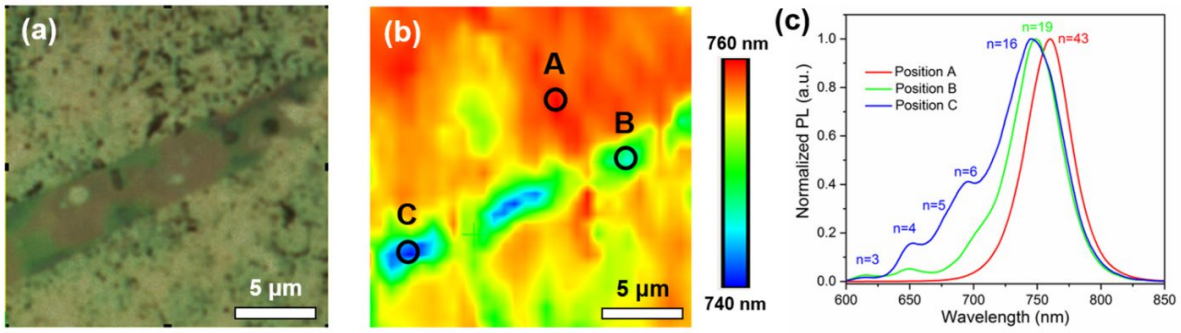

Figure 4. (**a**) Optical microscopy images of the front surface of 12 mol% MACl layered perovskite film. (**b**) 2D distribution profiles of PL peak position corresponding to (**a**). (**c**) Normalized PL spectra of three selected positions labeled in (**b**).

Compared to the surface sensitive PL spectroscopic technique, absorption spectroscopy is a good indicator of the overall composition of perovskite films. **Figure S3** presents the UV-vis absorption spectra of layered perovskite films with various MACl doping ratios. Absorption peaks corresponding to the excitonic excitation of small-*n* (*n*=2, 3, 4, 5) 2D perovskite components can be identified for all film samples. The gradual enhancement of these peaks with the increase of MACl doping ratio can be ascribed to the increased amount of small-*n* 2D perovskite components in MACl doped films. At the same time, the absorbance in the long wavelength region corresponding to large-*n* 2D perovskite decreases upon increased MACl doping. As the quantity of spacer BA cations is constant, this observation can be explained as the amount of small-*n* component increasing at the expense of a reduced amount and increased thickness of large-*n* 2D perovskite. Combined with the PL characterization results, we propose that MACl can facilitate the formation of small-*n* 2D $BA_2MA_{n-1}Pb_nI_{3n+1}$ perovskites by cationic substitution similar to the case in 3D perovskite.[31] As

described in **Equations 4a&b**, the formation of $BA_2MA_{n-1}I_{3n+1} \cdot xMACl$ (x is the initial MACl doping ratio) intermediate phase followed by the cationic substitution of BA to MA and the release of MACl occurs during the casting and annealing of layered perovskite film at 100 °C.

$$nPbI_2 + 2BAI + (n-1)MAI + xMACl \rightarrow BA_2MA_{n-1}Pb_nI_{3n+1} \cdot xMACl \quad (4a)$$

$$BA_2MA_{n-1}Pb_nI_{3n+1} \cdot xMACl \xrightarrow{Annealing} BA_2MA_{n-1}Pb_nI_{3n+1} + xMACl\uparrow \quad (4b)$$

Ultrafast transient absorption (TA) measurements were also carried out to probe the compositional change of layered perovskite films upon MACl doping. The pseudo-color 2D representations of the TA spectra measured following 510 nm excitation for both front-side and back-side excitation (transmitted probe detection) modes for 0 mol% and 6 mol% MACl films are shown in **Figure 5a&b, d&e**, while spectra for the other films are given in **Figure S6**. Distinct ground state bleaching (GB) peaks corresponding to small-*n* and large-*n* perovskite components can be easily recognized in the TA spectra obtained by back-side excitation. The positive weak and broad signal at wavelengths shorter than 600 nm can be assigned to the derivative feature resulting from the blue-shift of the band edge exciton resonance predominantly from the *n*=3 phase.[32] The compositional differences between films with various MACl doping obtained by back- and front-side excitation are made clear when the TA spectra are compared at 5 ps, as shown in **Figure 5c&f**. With the increase of MACl doping, a gradual enhancement of the GB peaks of small-*n* 2D perovskites together with a decrease of the GB peak of large-*n* 2D perovskite obtained from back-side excitation are consistent with the UV-vis spectra, further strengthening the view that the amount of small-*n* 2D perovskites increases at the cost of reducing the large-*n* 2D perovskite. By comparing the TA spectra obtained from the back and front-side excitation, it can be confirmed that small-*n* 2D perovskite components are more concentrated at the back side of the film without MACl doping, which emerge onto the front side of the film upon MACl doping.

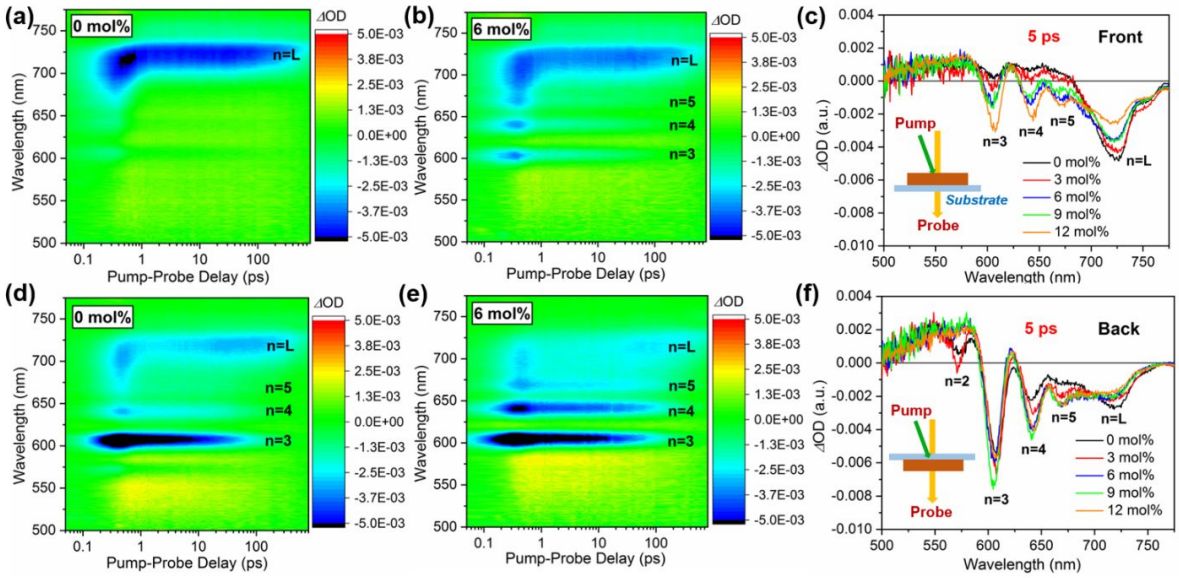

Figure 5. (**a&b**) Pseudo-color 2D TA spectra of 0 mol% (**a**) and 6 mol% MACl (**b**) layered perovskite films obtained with front-side excitation. (**d&e**) Pseudo-color 2D TA spectra of 0 mol% (**d**) and 6 mol% (**e**) MACl layered perovskite films obtained with back-side excitation. (**c&f**) TA spectra of 0 mol%, 3 mol%, 6 mol%, 9 mol%, 12 mol% MACl layered perovskite films as a function of probe wavelength obtained with front-side (**c**) and back-side (**f**) excitation taken at 5ps delays (Insets are the measurement configurations). (λ_{ex}=510 nm)

To obtain the dynamics of excitons in layered perovskite films without and with MACl additives, the TA signal as a function of pump-probe delay (horizontal cut) at wavelengths of each GB peak for 0 mol% and 6 mol% MACl films obtained from back side excitation are plotted in **Figure 6a&b**. A biexponential decay function expressed by:

$$I(t) = I_0 + A_1 \exp\left(-\frac{t-t_0}{\tau_1}\right) + A_2 \exp\left(-\frac{t-t_0}{\tau_2}\right) \quad (5)$$

gave the best fit for all decay profiles. As summarized in **Table 1**, fit parameters indicate that decay profiles of small-*n* phases (*n*=3, 4, 5) are described by a sub-ps scale fast decay component and a slow decay component of tens of picoseconds. The fast decay is attributed to exciton-exciton annihilation while the relatively slow decay can be assigned to a combined process for exciton decay, including radiative recombination, trap state filling, and energy transfer to the large-n perovskite phase.[33] The decreased ratio of the exciton annihilation decay channel (A_1%) as well as the increased decay time constant (τ_2) for all small-*n* phases upon MACl doping is an indicator of a more ordered spacer cation arrangement and fewer defects for small-*n* 2D perovskites in the 6 mol% MACl film compared to other films. The kinetic profile of the GB peak corresponding to large-*n* (*n*=L) perovskite is composed of an increasing component and a slow decay channel that occurs on the nanosecond timescale. As the long lifetime decay constant (τ_2) is

beyond the time window of our measurement (900 ps), it was arbitrarily fixed at 10 ns to allow the fitting of the fast rising component for both film samples. The rise of the GB signal has been previously assigned as being due to the progressive population of excitons in the large-*n* perovskite phase due to energy transfer from small-*n* perovskites.[34] The higher ratio of this rising component (64.4%) for the 6 mol% MACl film compared to that of the 0 mol% MACl film (47.6%) implies the energy cascade from small-*n* to large-*n* phases becomes more prominent upon MACl doping,[35] which would be beneficial for the effective funneling and collection of charge carriers required for high photovoltaic performance in PSC devices.

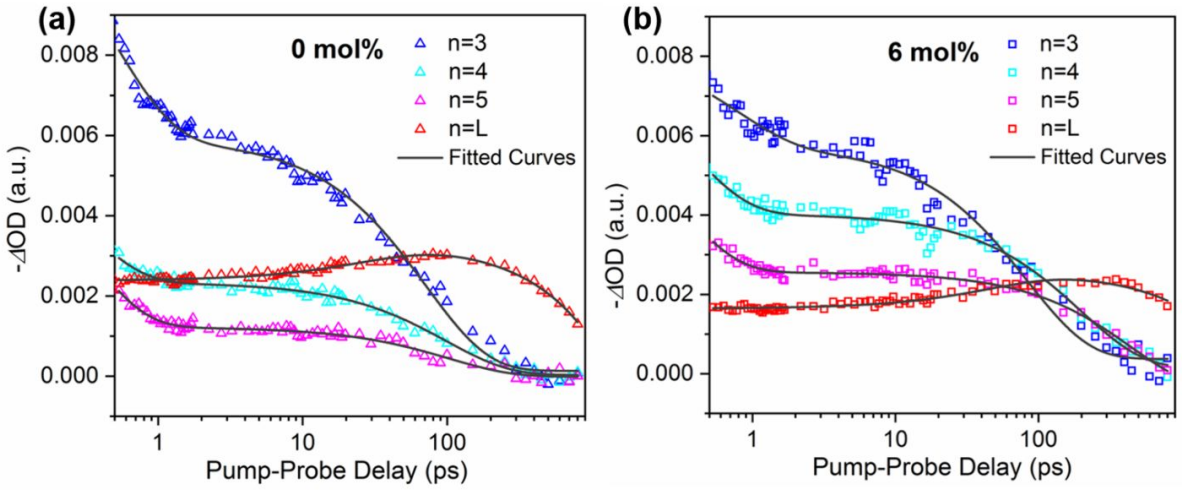

Figure 6. Plotted decay profiles of indicated GB peaks (-ΔOD) as a function of pump-probe delay and corresponding fitted curves for 0 mol% MACl (**a**) and 6 mol% MACl (**b**) layered perovskite films with back-side excitation.

Table 1. Fitting parameters for decay profiles of GB peaks in 0 mol% MACl and 6 mol% MACl films.

	0 mol% MACl				6 mol% MACl			
	A_1%	τ_1 (ps)	A_2%	τ_2 (ps)	A_1%	τ_1 (ps)	A_2%	τ_2 (ps)
n=3	38.3	0.47	61.7	71.1	19.7	0.76	80.3	83.6
n=4	52.1	0.28	47.9	98.4	8.5	0.35	91.4	199.3
n=5	31.9	0.26	68.1	103.0	2.9	0.29	97.1	448.5
n=L	47.6	29.9	52.4	10 ns	64.4	51.4	35.6	10 ns

*A_1%=$|A_1|/(|A_1|+|A_2|)$; A_2%=$|A_2|/(|A_1|+|A_2|)$; Note: for *n*=L decay profiles, $A_1<0$.

Time-resolved PL (TRPL) measurements were carried out to investigate charge carrier dynamics both in the individual layered perovskite films and the perovskite/electron transporting layer interface. **Figures 7a&b** show the normalized TRPL spectra of all five film samples covered by insulating PMMA layers (without PCBM) and by electron transporting PCBM layers measured from the front surface using the reflection acquisition mode. For the convenience of comparison, only PL emission from the large-n 2D component was detected for all films. A bi-exponential decay function was adopted to fit all TRPL decay

profiles, and provided the amplitude average lifetimes of charge carriers for layered perovskite films without PCBM ($\tau_{w/o}$) and with a PCBM (τ_{with}) coating layer. As summarized in **Table 2**, the variation of $\tau_{w/o}$ with MACl doping ratio shows a tendency to first increase (from 0 mol% to 9 mol%) and then decrease (from 9 mol% to 12 mol%), which corresponds with the PL intensity shown in **Figure 3b**. Both increased crystallinity of the large-*n* perovskite phase and decreased density of trap states can contribute to the increase of carrier lifetime. Considering the larger thickness of large-*n* 2D perovskite for the 12 mol% MACl film compared to the 9 mol% MACl sample, the observed short carrier lifetime for the former can be explained by the decreased passivation effect provided by small-*n* 2D perovskites caused by the self-aggregation, similar to the situation highlighted in the mixed 3D/2D hybrid perovskite structures.[36, 37] In the perovskite/PCBM bilayer films, photo-generated electrons in layered perovskite films can be transferred to the PCBM layer owing to the offset of LUMO levels, which is one of the critical principles for the operation of PSC devices. The feasibility of this interfacial charge transfer process can be characterized by the electron transfer rate (k_{ET}) calculated by:[25]

$$k_{ET} = \frac{1}{\tau_{with}} - \frac{1}{\tau_{w/o}} \quad (6)$$

As shown in **Table 2**, with the increase of MACl doping ratio from 0 mol% to 12 mol%, k_{ET} increases first and then decreases, achieving the maximum value of $8.78 \times 10^8\ s^{-1}$ for the 6 mol% MACl sample, nearly twice that for the undoped film ($4.41 \times 10^8\ s^{-1}$). A large k_{ET} is beneficial for charge collection by the electrode in PSC devices and contributes to high photovoltaic performance. This result is in accordance with the highest PCE for a PSC based on 6 mol% MACl doped layered perovskite film. Although the 9 mol% MACl film possesses a higher charge carrier lifetime than the 6 mol% sample, the k_{ET} for the 9 mol% film is reduced. This can be explained by the increased surface roughness for layered perovskite films with MACl doping as revealed by the SEM images (**Figure S7**). As shown in **Figure S7a**, the front surface of the 0 mol% MACl film exhibits smooth and uniform grains of a few microns in size. However, features attributed to the sharp edges of small-*n* perovskite flakes appear on the surface of the 6 mol% MACl and 9 mol% MACl films (**Figure S7c&d**), indicating an increased roughness of layered perovskite films with the increase of MACl doping ratio. This is disadvantageous for the close contact and effective electron transfer between the perovskite film and the PCBM layer, inferring that high MACl doping can be a negative factor for PSC performance from the interfacial morphology perspective. Thus, the competitive effects of passivation of defects and roughness increase, induced by MACl doping, lead to the highest PCE for a PSC device being achieved for 6 mol% MACl doping.

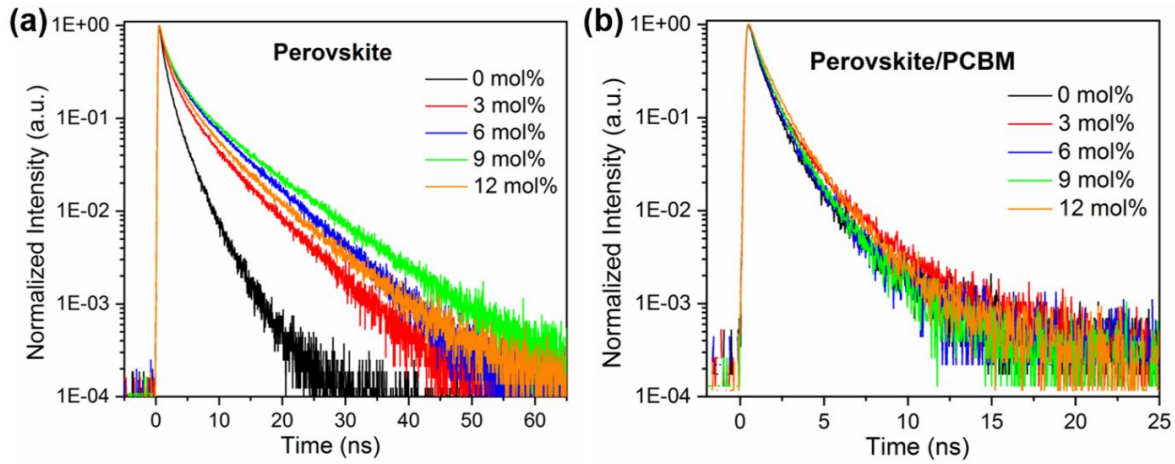

Figure 7. TRPL of 0 mol%, 3 mol%, 6 mol%, 9 mol%, 12 mol% MACl layered perovskite films without (**a**) and with (**b**) a PCBM layer.

Table 2. Fitted average PL lifetimes for layered perovskite films without PCBM ($\tau_{w/o}$) and with PCBM (τ_{with}) coating layer, and the derived electron transfer rate (k_{ET}).

	0 mol%	3 mol%	6 mol%	9 mol%	12 mol%
$\tau_{w/o}$ (ps)	1172	2140	2794	3076	2478
τ_{with} (ps)	7723	895	809	890	1002
k_{ET} ($\times 10^8 s^{-1}$)	4.41	6.51	8.78	7.99	5.94

Powder X-ray diffraction (XRD) was applied to investigate the crystallographic information from the front surface of layered perovskite films. In the diffraction data presented in **Figure 8a**, diffraction peaks assigned to the (101), (202), (0k0) lattice planes of large-n 2D perovskite phase can be recognized for all films.[14] Diffraction peaks with low diffraction angle (6.7°) emerging at 9 mol% and 12 mol% MACl films are the (0k0) diffraction peaks of small-n perovskite phase present at the front surface.[9] As schematically illustrated in the inset, the (101) and (202) planes ([101] crystal orientation) are perpendicular (parallel) to the 2D perovskite layer, while the (0k0) plane ([010] crystal orientation) is parallel to the 2D perovskite layer. As the diffraction peak intensity is proportional to the weight fraction of a phase, the adjacent (202) and (0k0) peaks of large-*n* perovskite are selected to quantify the fraction of 2D perovskite phase aligned perpendicular to the substrate using:

$$f_{[101]} = \frac{I_{(202)}}{I_{(202)} + I_{(0k0)}} \quad (7)$$

in which $I_{(202)}$ and $I_{(0k0)}$ are the corresponding peak intensities.[38] The gradual increase of the (202) peak intensity with respect to the (0k0) peak with increasing MACl doping ratio leads to an increase of $f_{[101]}$

from 0.42 for 0 mol% MACl film to 0.83 for 12 mol% MACl film, as plotted in **Figure 8b**, indicating an increased amount of [101] oriented large-*n* 2D perovskite layers in the orthogonal direction. Furthermore, the (101) diffraction peak is adopted to estimate the average crystal size (*D*) of 2D perovskite layers based on the Scherrer Equation:

$$D = \frac{0.89 \cdot \lambda}{\beta \cdot cos\theta} \quad (8)$$

where λ is the wavelength of the X-ray, β is the full width half maximum (FWHM) of the diffraction peak and θ is the diffraction peak position.[39] As depicted in **Figure 8b**, the average crystal size for the large-*n* perovskite phase increases from 23 nm for the un-doped film to 28 nm for the film with 12 mol% MACl doping. Considering the consistency of crystal size and layer thickness of the large-n perovskite phase, an increase of layer thickness upon MACl doping is further verified. By dividing *D* by the thickness of a single PbI_6^{4-} layer (0.632nm),[40] the layer thickness of large-*n* 2D perovskite layer in 12 mol% MACl film is estimated to be 44, closely matching the value (*n*=42) obtained through the excitonic gap calculation. This observation is in accordance with the finding that a 2D perovskite flake tends to be aligned more perpendicular to the substrate with increasing *n* from 1 to 4.[38] Thus, as schematically illustrated in **Figure 8c**, an increasing population of the perpendicularly aligned large-*n* 2D perovskite phase in the layered perovskite film resulted from the increasing thickness of the large-*n* 2D perovskite layer upon MACl doping is revealed.

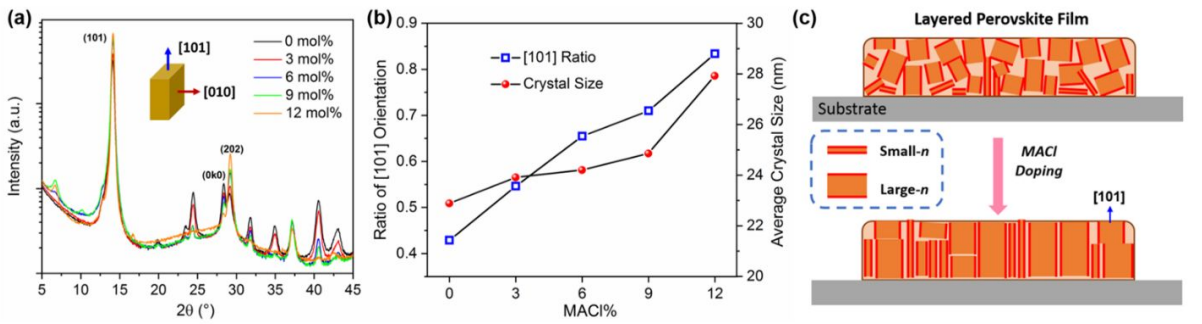

Figure 8. (**a**) XRD patterns of 0 mol%, 3 mol%, 6 mol%, 9 mol%, 12 mol% MACl layered perovskite films (Intensity is displayed on a $\log_{10}$ scale). (**b**) Plots of [101] crystal orientation ratio and average crystal size of large-*n* 2D perovskite phase in layered perovskite films against MACl doping ratio. (**c**) Schematic diagram of the structural variation of layered perovskite films upon MACl doping.

CONCLUSIONS

A systematic investigation was carried out to uncover the structural and compositional variation of <*n*>=5 layered perovskite films with varying amounts of MACl doping. We emphasize that the commonly believed 3D-like perovskite phase observed in the layered perovskite film is more accurately labelled large-*n* 2D perovskite flakes, with the thickness increasing from *n*=18 for an un-doped (0 mol% MACl) layered

perovskite film to *n*=42 for a 12 mol% MACl film. It is proposed that MACl additives facilitate the crystallization of small-*n* perovskites, leading to consumption of spacer cations and thus an increased thickness of large-*n* perovskite flakes. The decreased defect density and improved crystallinity for the large-*n* perovskite phase owing to the passivation effect provided by small-*n* perovskites, together with the increased tendency for orthogonal alignment of large-*n* perovskite flakes relative to the substrate, are responsible for the PCE enhancement of PSC devices with increasing MACl doping ratio. However, the increased roughness of the film front surface resulting from the sharp edges of small-*n* perovskite flakes is detrimental to efficient electron transfer from the perovskite film to the adjacent electron transporting layer, leading to a compromise that PSC devices with 6 mol% MACl doping exhibit the highest PCE of ~14.3%.

This research provides new insight into the structure and composition of layered 2D perovskite films and reveals the mechanism of performance enhancement of PSC devices upon MACl doping. These findings should be of significance for the further performance improvement of 2D PSCs and also for the exploration of 2D Ruddlesden-Popper perovskites in other optoelectronic applications.

EXPERIMENTAL SECTION

Materials. Lead iodide (PbI_2) was purchased from Alfa Aesar. Methylammonium iodide (MAI), butylammonium iodide (BAI), methylammonium chloride (MACl), were provided by Greatcell Solar. Anhydrous dimethylformamide (DMF), chloroform ($CHCl_3$) aqueous hydriodic acid (HI, 57 wt. %), hypophosphorous acid solution (H_3PO_2, 50 wt. % in H_2O) were purchased from Sigma Aldrich, Australia. All chemicals were used as received without further purification.

Synthesis of 2D perovskite single crystals. 2D perovskite single crystals with *n*=1, 2, 3, 4, 5 and 3D (*n*=∞) $MAPbI_3$ were synthesized by the supersaturation method reported before with some modification.[9] 1 mmol (460.8 mg) PbI_2 was dissolved into a 1.17 ml HI/H_3PO_2 (v/v=1: 0.17) aqueous mixture. To synthesize 2D *n*=1 (BA_2PbI_4) perovskite, 2 mmol (401.8 mg) BAI was added to the mixed solution by heating to 95 °C under constant magnetic stirring for 10 mins, leading to the formation of a clear bright yellow solution. For the synthesis of *n*=2, *n*=3, *n*=4, *n*=5, *n*=∞ (3D) perovskites, the ammonium salts were added as follows; 1 mmol BAI/0.5 mmol MAI, 0.667 mmol BAI/0.667 mmol MAI, 0.5 mmol BAI/0.75 mmol MAI, 0.4 mmol BAI/0.8 mmol MAI, 1 mmol MAI, respectively. These hot solutions were left to cool to room temperature overnight for the growth of crystals. All the 2D perovskite crystals formed in solutions were collected by filtration and were dried in a vacuum oven.

Film preparation. 2.4 mmol PbI_2, 0.96 mmol BAI, 1.92 mmol MAI were dissolved into 2 ml DMF with magnetic stirring on a 70 °C hot plate for 30 mins, forming a 1.2 M (with respect to Pb^{2+}) stock precursor

solution of <*n*>=5 perovskite. 5 separate 400 μL precursor solutions (1.2 M) were diluted to 0.3 M by adding stoichiometric amounts of pure DMF and 0.1 M MACl solution (DMF) to obtain the precursors of 2D $BA_2MA_4Pb_5I_{16}$ perovskite doped with 0 mol%, 3 mol%, 6 mol%, 9 mol%, 12 mol% MACl. Layered perovskite (<*n*>=5) films were deposited from these precursor solutions by the one-step drop-casting method.[23] 5 μL precursor was dropped onto the center of a clear glass substrate (2.5 cm × 2.5 cm), which was placed on a 60 °C hot plate, that spread out to form a circular film after the evaporation of DMF. Afterwards, the film was transferred to a 100 °C hot plate for 2 minutes of annealing. Films for TRPL measurements were coated by PMMA or PCBM layers through spin-coating by addition of PMMA (10 mg/ml) or PCBM (10 mg/ml) $CHCl_3$ solution at 1000 rpm for 30 s.

Device fabrication and characterizations. Pre-patterned ITO glass plates were sequentially cleaned by ultrasound sonication in detergent, deionized water, acetone, isopropyl alcohol for 5 mins, successively. After 15 minutes of UV ozone treatment, a PEDOT:PSS hole transporting layer (HTL) was added by spin coating at 5000 rpm followed by 15 minutes of annealing at 140 °C. Layered perovskite films were deposited by the one-step drop-casting method. A PCBM electron transporting layer and polyethylenimine ethoxylated (PEIE) interfacial layer were then sequentially spin coated on the top of the layered perovskite films using PCBM (10 mg/ml in $CHCl_3$) solution and PEIE (0.05% w/w in isopropanol) solution at 1000 rpm for 30 s and 4000 rpm for 30 s, respectively. A 100 nm Ag layer was then added by thermal evaporation through a shadow mask, giving a PSC device with the structure of ITO/PEDOT:PSS/Layered Perovskite/PCBM/PEIE/Ag with an active area of 0.1 cm^2. Current density-Voltage (J-V) curves of PSCs based on layered perovskite films with various ratios of MACl doping were measured using a Keithley 2400 Source Meter with a scan rate of 100 mV/s under standard solar illumination (AM 1.5G, 100 $mW \cdot cm^{-2}$). 10 sets of devices were measured for averaging the performance parameters. The maximum power output (MPP) curves for 0 mol% MACl and 6 mol% MACl PSC devices were recorded under the same conditions.

General characterizations. The UV−vis absorption spectra of the sample films were collected using a UV−Visible spectrophotometer (CARY 50 Bio, Varian). Steady-state PL spectra was acquired by focusing 405 nm laser excitation (PDL 800-D, PICO QUANT Inc.) onto the film surface through a 5× objective, giving a laser spot size of ~100 μm in diameter, with PL emission signals recorded by a Si-CCD detector-based spectrometer (Avantas Inc.). Powder X-ray diffraction measurements of layered perovskite films with various MACl doping were performed using a Rigaku SmartLab X-ray diffractometer with X-ray wavelength of λ=1.542 Å generated by Cu K_α emission. A scanning electron microscope (FEI Teneo) was used to obtain the SEM images of the layered perovskite front surfaces. Elemental investigations of

perovskite films were carried out by the energy dispersive X-ray (EDX) analysis system attached to the SEM instrument.

Fluorescence microscopy. Optical microscopy images of all layered perovskite films placed on a piezoelectric scanning stage were obtained using a confocal optical microscope (Nanofinder FLEX2. Tokyo Instruments, Inc.). Spatially resolved fluorescence (PL) imaging of films was performed under the same microscope with 400 nm (80 MHz) excitation laser provided by a frequency doubled Ti-Sapphire femtosecond laser system and PL emission detected by a fiber connected spectrometer (MS454i, SDL Instruments). The spatial resolution of the piezoelectric scanning stage for PL mapping is ~300 nm in the horizontal direction.

Time resolved photoluminescence spectroscopy. TRPL of all film samples was measured through a confocal microscope (Olympus, IX71/FV300), equipped with a TCSPC setup. The 400 nm excitation beam was the frequency doubled output of a mode-locked and cavity dumped Ti:Sapphire laser (Coherent Mira900f/APE PulseSwitch, 1 MHz, 100 fs FWHM) which was focused on the front surface of films through a 10× objective lens. The PL emission was collected by the same objective lens and detected confocally by a single photon counting photomultiplier (Becker & Hickl, PMC-100-1), following an appropriate highpass filter. Time-resolved PL images were recorded using a commercial photon counting system (SPC150 card, Becker & Hickl, Germany). The instrument response function of this system is ~200 ps, limited by the transit time spread of the photomultiplier used.

Transient absorption spectroscopy. The 800 nm pulsed output (96 KHz, 60 fs FWHM) generated by a high repetition rate amplifier (Coherent RegA9050) was split to generate the pump (510 nm) beam through a tunable optical parametric amplifier (Coherent OPA9450) and the probe (near-IR white light) beam using a 3-mm-thick sapphire window (CASTECH), respectively. Pump and probe pulses were focused by an off-axis parabolic reflector to overlap at the surface of the film sample with a pump spot size of ~200 μm, giving an excitation fluence of 0.52 $\mu J \cdot cm^{-2}$. Pump induced absorption changes (ΔOD) were measured by comparing adjacent transmitted probe pulses with and without pump pulses using a synchronized mechanical chopper in the path of the pump beam. The time-resolved transient absorption spectra were recorded using a high-speed fiber-optic spectrometer (Ultrafast Systems). The temporal resolution of the setup was estimated to be 200 fs FWHM.

ASSOCIATED CONTENT

Supporting Information

The Supporting Information is available free of charge at XXXXXX

Photographs of 2D $BA_2MA_{n-1}Pb_nI_{3n+1}$ crystals and <*n*>=5 layered perovskite film; PCE stability of 6 mol% MACl based 2D PSC device; UV-vis absorption spectra of layered perovskite films doped with 0 mol%, 3 mol%, 6 mol%, 9 mol%, 12 mol% MACl additive; EDX spectrum of 0 mol% and 6 mol% MACl layered perovskite films; Optical microscopy images of layered perovskite films with various MACl doping ratio; TA spectra of 3 mol%, 9 mol%, 12 mol% MACl layered perovskite films obtained with front-side and back-side excitation; SEM images of layered perovskite films with various MACl doping ratio. EQE spectrum of 2D PSC.

AUTHOR INFORMATION

Corresponding Authors

Kenneth P. Ghiggino − *School of Chemistry and ARC Centre of Excellence in Exciton Science, The University of Melbourne, Parkville, Victoria 3010, Australia*; Email: ghiggino@unimelb.edu.au

Mei Gao – *Flexible Electronics Laboratory, CSIRO Manufacturing, Clayton, VIC 3168, Australia*; Email: Mei.Gao@csiro.au

Authors

Fei Zheng − *School of Chemistry and ARC Centre of Excellence in Exciton Science, The University of Melbourne, Parkville, Victoria 3010, Australia*

Chuantian Zuo − *Flexible Electronics Laboratory, CSIRO Manufacturing, Clayton, VIC 3168, Australia*

Mengsi Niu − *School of Physics, State Key Laboratory of Crystal Materials, Shandong University, Jinan 250100, Shandong, China*

Chunhua Zhou − *Centre for Translational Atomaterials, Swinburne University of Technology, Hawthorn, Victoria 3122, Australia*

Siobhan J. Bradley − *School of Chemistry and ARC Centre of Excellence in Exciton Science, The University of Melbourne, Parkville, Victoria 3010, Australia*

Christopher R. Hall − *School of Chemistry and ARC Centre of Excellence in Exciton Science, The University of Melbourne, Parkville, Victoria 3010, Australia*

Weilong Xu − *School of Chemistry and ARC Centre of Excellence in Exciton Science, The University of Melbourne, Parkville, Victoria 3010, Australia*

Xiaoming Wen − *Centre for Translational Atomaterials, Swinburne University of Technology, Hawthorn, Victoria 3122, Australia*

Xiaotao Hao − *School of Physics, State Key Laboratory of Crystal Materials, Shandong University, Jinan 250100, Shandong, China*; *School of Chemistry and ARC Centre of Excellence in Exciton Science, The University of Melbourne, Parkville, Victoria 3010, Australia*

Trevor A. Smith − *School of Chemistry and ARC Centre of Excellence in Exciton Science, The University of Melbourne, Parkville, Victoria 3010, Australia*

Notes

The authors declare no conflicts of interest.

ACKNOWLEDGMENTS

The authors acknowledge funding support from the ARC Centre of Excellence in Exciton Science (CE170100026).

REFERENCES

(1) Tsai, H.; Nie, W.; Blancon, J. C.; Stoumpos, C. C.; Asadpour, R.; Harutyunyan, B.; Neukirch, A. J.; Verduzco, R.; Crochet, J. J.; Tretiak, S.; Pedesseau, L.; Even, J.; Alam, M. A.; Gupta, G.; Lou, J.; Ajayan, P. M.; Bedzyk, M. J.; Kanatzidis, M. G., High-Efficiency Two-Dimensional Ruddlesden-Popper Perovskite Solar Cells. *Nature* **2016,** *536*, 312-316.

(2) Tian, H.; Zhao, L.; Wang, X.; Yeh, Y. W.; Yao, N.; Rand, B. P.; Ren, T. L., Extremely Low Operating Current Resistive Memory Based on Exfoliated 2D Perovskite Single Crystals for Neuromorphic Computing. *ACS Nano* **2017,** *11*, 12247-12256.

(3) Wang, K.; Wu, C.; Yang, D.; Jiang, Y.; Priya, S., Quasi-Two-Dimensional Halide Perovskite Single Crystal Photodetector. *ACS Nano* **2018,** *12*, 4919-4929.

(4) Thouin, F.; Valverde-Chavez, D. A.; Quarti, C.; Cortecchia, D.; Bargigia, I.; Beljonne, D.; Petrozza, A.; Silva, C.; Srimath Kandada, A. R., Phonon Coherences Reveal the Polaronic Character of Excitons in Two-Dimensional Lead Halide Perovskites. *Nat. Mater.* **2019,** *18*, 349-356.

(5) Cao, D. H.; Stoumpos, C. C.; Farha, O. K.; Hupp, J. T.; Kanatzidis, M. G., 2D Homologous Perovskites as Light-Absorbing Materials for Solar Cell Applications. *J. Am. Chem. Soc.* **2015,** *137*, 7843-50.

(6) Mauck, C. M.; Tisdale, W. A., Excitons in 2D Organic–Inorganic Halide Perovskites. *Trends in Chemistry* **2019,** *1*, 380-393.

(7) Quintero-Bermudez, R.; Gold-Parker, A.; Proppe, A. H.; Munir, R.; Yang, Z.; Kelley, S. O.; Amassian, A.; Toney, M. F.; Sargent, E. H., Compositional and Orientational Control in Metal Halide Perovskites of Reduced Dimensionality. *Nat. Mater.* **2018,** *17*, 900-907.

(8) Li, P.; Liang, C.; Liu, X. L.; Li, F.; Zhang, Y.; Liu, X. T.; Gu, H.; Hu, X.; Xing, G.; Tao, X.; Song, Y., Low-Dimensional Perovskites with Diammonium and Monoammonium Alternant Cations for High-Performance Photovoltaics. *Adv. Mater.* **2019**, 31, 1901966.

(9) Stoumpos, C. C.; Cao, D. H.; Clark, D. J.; Young, J.; Rondinelli, J. M.; Jang, J. I.; Hupp, J. T.; Kanatzidis, M. G., Ruddlesden–Popper Hybrid Lead Iodide Perovskite 2D Homologous Semiconductors. *Chem. Mater.* **2016,** *28*, 2852-2867.

(10) Thouin, F.; Neutzner, S.; Cortecchia, D.; Dragomir, V. A.; Soci, C.; Salim, T.; Lam, Y. M.; Leonelli, R.; Petrozza, A.; Kandada, A. R. S.; Silva, C., Stable Biexcitons in Two-Dimensional Metal-Halide Perovskites with Strong Dynamic Lattice Disorder. *Phys. Rev. Mater.* **2018,** *2*, 034001.

(11) Chen, A. Z.; Shiu, M.; Ma, J. H.; Alpert, M. R.; Zhang, D.; Foley, B. J.; Smilgies, D. M.; Lee, S. H.; Choi, J. J., Origin of Vertical Orientation in Two-Dimensional Metal Halide Perovskites and its Effect on Photovoltaic Performance. *Nat. Commun.* **2018,** *9*, 1336.

(12) Lin, Y.; Fang, Y.; Zhao, J.; Shao, Y.; Stuard, S. J.; Nahid, M. M.; Ade, H.; Wang, Q.; Shield, J. E.; Zhou, N.; Moran, A. M.; Huang, J., Unveiling the Operation Mechanism of Layered Perovskite Solar Cells. *Nat. Commun.* **2019,** *10*, 1008.
(13) Hu, J.; Oswald, I. W. H.; Stuard, S. J.; Nahid, M. M.; Zhou, N.; Williams, O. F.; Guo, Z.; Yan, L.; Hu, H.; Chen, Z.; Xiao, X.; Lin, Y.; Yang, Z.; Huang, J.; Moran, A. M.; Ade, H.; Neilson, J. R.; You, W., Synthetic Control over Orientational Degeneracy of Spacer Cations Enhances Solar Cell Efficiency in Two-Dimensional Perovskites. *Nat. Commun.* **2019,** *10*, 1276.
(14) Soe, C. M. M.; Nie, W.; Stoumpos, C. C.; Tsai, H.; Blancon, J.-C.; Liu, F.; Even, J.; Marks, T. J.; Mohite, A. D.; Kanatzidis, M. G., Understanding Film Formation Morphology and Orientation in High Member 2D Ruddlesden-Popper Perovskites for High-Efficiency Solar Cells. *Adv. Energy Mater.* **2018,** *8*, 1700979.
(15) Zhang, X.; Munir, R.; Xu, Z.; Liu, Y.; Tsai, H.; Nie, W.; Li, J.; Niu, T.; Smilgies, D. M.; Kanatzidis, M. G.; Mohite, A. D.; Zhao, K.; Amassian, A.; Liu, S. F., Phase Transition Control for High Performance Ruddlesden-Popper Perovskite Solar Cells. *Adv. Mater.* **2018**, 30, 1707166.
(16) Lai, H.; Kan, B.; Liu, T.; Zheng, N.; Xie, Z.; Zhou, T.; Wan, X.; Zhang, X.; Liu, Y.; Chen, Y., Two-Dimensional Ruddlesden-Popper Perovskite with Nanorod-like Morphology for Solar Cells with Efficiency Exceeding 15%. *J. Am. Chem. Soc.* **2018,** *140*, 11639-11646.
(17) Dar, M. I.; Arora, N.; Gao, P.; Ahmad, S.; Gratzel, M.; Nazeeruddin, M. K., Investigation Regarding the Role of Chloride in Organic-Inorganic Halide Perovskites Obtained from Chloride Containing Precursors. *Nano Lett.* **2014,** *14*, 6991-6996.
(18) Qing, J.; Liu, X.-K.; Li, M.; Liu, F.; Yuan, Z.; Tiukalova, E.; Yan, Z.; Duchamp, M.; Chen, S.; Wang, Y.; Bai, S.; Liu, J.-M.; Snaith, H. J.; Lee, C.-S.; Sum, T. C.; Gao, F., Aligned and Graded Type-II Ruddlesden-Popper Perovskite Films for Efficient Solar Cells. *Adv. Energy Mater.* **2018,** *8*, 1800185.
(19) Chen, H.; Xia, Y.; Wu, B.; Liu, F.; Niu, T.; Chao, L.; Xing, G.; Sum, T.; Chen, Y.; Huang, W., Critical Role of Chloride in Organic Ammonium Spacer on the Performance of Low-Dimensional Ruddlesden-Popper Perovskite Solar Cells. *Nano Energy* **2019,** *56*, 373-381.
(20) Kim, M.; Kim, G.-H.; Lee, T. K.; Choi, I. W.; Choi, H. W.; Jo, Y.; Yoon, Y. J.; Kim, J. W.; Lee, J.; Huh, D.; Lee, H.; Kwak, S. K.; Kim, J. Y.; Kim, D. S., Methylammonium Chloride Induces Intermediate Phase Stabilization for Efficient Perovskite Solar Cells. *Joule* **2019,** *3*, 2179-2192.
(21) Liu, Y.; Ye, H.; Zhang, Y.; Zhao, K.; Yang, Z.; Yuan, Y.; Wu, H.; Zhao, G.; Yang, Z.; Tang, J.; Xu, Z.; Liu, S., Surface-Tension-Controlled Crystallization for High-Quality 2D Perovskite Single Crystals for Ultrahigh Photodetection. *Matter* **2019,** *1*, 465-480.
(22) Zheng, F.; Xu, W.-L.; Jin, H.-D.; Hao, X.-T.; Ghiggino, K. P., Charge Transfer from Poly(3-hexylthiophene) to Graphene Oxide and Reduced Graphene Oxide. *RSC Adv.* **2015,** *5*, 89515-89520.
(23) Zuo, C.; Scully, A. D.; Vak, D.; Tan, W.; Jiao, X.; McNeill, C. R.; Angmo, D.; Ding, L.; Gao, M., Self-Assembled 2D Perovskite Layers for Efficient Printable Solar Cells. *Adv. Energy Mater.* **2019,** *9*, 1803258.
(24) Pazoki, M.; Jacobsson, T. J.; Cruz, S. H. T.; Johansson, M. B.; Imani, R.; Kullgren, J.; Hagfeldt, A.; Johansson, E. M. J.; Edvinsson, T.; Boschloo, G., Photon Energy-Dependent Hysteresis Effects in Lead Halide Perovskite Materials. *J. Phys. Chem. C* **2017,** *121*, 26180-26187.
(25) Zheng, F.; Wen, X.; Bu, T.; Chen, S.; Yang, J.; Chen, W.; Huang, F.; Cheng, Y.; Jia, B., Slow Response of Carrier Dynamics in Perovskite Interface Upon Illumination. *ACS Appl. Mater. Interfaces* **2018,** *10*, 31452-31461.
(26) Huang, Z.; Proppe, A. H.; Tan, H.; Saidaminov, M. I.; Tan, F.; Mei, A.; Tan, C.-S.; Wei, M.; Hou, Y.; Han, H.; Kelley, S. O.; Sargent, E. H., Suppressed Ion Migration in Reduced-Dimensional Perovskites Improves Operating Stability. *ACS Energy Lett.* **2019,** *4*, 1521-1527.
(27) Luo, T.; Zhang, Y.; Xu, Z.; Niu, T.; Wen, J.; Lu, J.; Jin, S.; Liu, S. F.; Zhao, K., Compositional Control in 2D Perovskites with Alternating Cations in the Interlayer Space for Photovoltaics with Efficiency Over 18%. *Adv. Mater.* **2019**, 31, 1903848.

(28) Zheng, F.; Chen, W.; Bu, T.; Ghiggino, K. P.; Huang, F.; Cheng, Y.; Tapping, P.; Kee, T. W.; Jia, B.; Wen, X., Triggering the Passivation Effect of Potassium Doping in Mixed-Cation Mixed-Halide Perovskite by Light Illumination. *Adv. Energy Mater.* **2019,** *9*, 1901016.
(29) Jang, D. M.; Park, K.; Kim, D. H.; Park, J.; Shojaei, F.; Kang, H. S.; Ahn, J. P.; Lee, J. W.; Song, J. K., Reversible Halide Exchange Reaction of Organometal Trihalide Perovskite Colloidal Nanocrystals for Full-Range Band Gap Tuning. *Nano Lett.* **2015,** *15*, 5191-5199.
(30) Li, J.; Wang, J.; Ma, J.; Shen, H.; Li, L.; Duan, X.; Li, D., Self-Trapped State Enabled Filterless Narrowband Photodetections in 2D Layered Perovskite Single Crystals. *Nat. Commun.* **2019,** *10*, No. 806.
(31) Mu, C.; Pan, J.; Feng, S.; Li, Q.; Xu, D., Quantitative Doping of Chlorine in Formamidinium Lead Trihalide ($FAPbI_{3-x}Cl_x$) for Planar Heterojunction Perovskite Solar Cells. *Adv. Energy Mater.* **2016,** *7*, 1601297.
(32) Wu, X.; Trinh, M. T.; Zhu, X. Y., Excitonic Many-Body Interactions in Two-Dimensional Lead Iodide Perovskite Quantum Wells. *J. Phys. Chem. C* **2015,** *119*, 14714-14721.
(33) Gan, Z.; Wen, X.; Zhou, C.; Chen, W.; Zheng, F.; Yang, S.; Davis, J. A.; Tapping, P. C.; Kee, T. W.; Zhang, H.; Jia, B., Transient Energy Reservoir in 2D Perovskites. *Adv. Opt. Mater.* **2019,** *7*, 1900971.
(34) Liu, J.; Leng, J.; Wu, K.; Zhang, J.; Jin, S., Observation of Internal Photoinduced Electron and Hole Separation in Hybrid Two-Dimentional Perovskite Films. *J. Am. Chem. Soc.* **2017,** *139*, 1432-1435.
(35) Yuan, M.; Quan, L. N.; Comin, R.; Walters, G.; Sabatini, R.; Voznyy, O.; Hoogland, S.; Zhao, Y.; Beauregard, E. M.; Kanjanaboos, P.; Lu, Z.; Kim, D. H.; Sargent, E. H., Perovskite Energy Funnels for Efficient Light-Emitting Diodes. *Nat. Nanotechnol.* **2016,** *11*, 872-877.
(36) Wang, Z.; Lin, Q.; Chmiel, F. P.; Sakai, N.; Herz, L. M.; Snaith, H. J., Efficient Ambient-Air-Stable Solar Cells with 2D–3D Heterostructured Butylammonium-Caesium-Formamidinium Lead Halide Perovskites. *Nat. Energy* **2017,** *2*, 1-10.
(37) Cho, Y.; Soufiani, A. M.; Yun, J. S.; Kim, J.; Lee, D. S.; Seidel, J.; Deng, X.; Green, M. A.; Huang, S.; Ho-Baillie, A. W. Y., Mixed 3D-2D Passivation Treatment for Mixed-Cation Lead Mixed-Halide Perovskite Solar Cells for Higher Efficiency and Better Stability. *Adv. Energy Mater.* **2018,** *8*, 1703392.
(38) Venkatesan, N. R.; Labram, J. G.; Chabinyc, M. L., Charge-Carrier Dynamics and Crystalline Texture of Layered Ruddlesden–Popper Hybrid Lead Iodide Perovskite Thin Films. *ACS Energy Lett.* **2018,** *3*, 380-386.
(39) Muniz, F. T. L.; Miranda, M. A. R.; Morilla dos Santos, C.; Sasaki, J. M., The Scherrer Equation and the Dynamical Theory of X-ray Diffraction. *Acta Cryst.* **2016,** *A72*, 385-390.
(40) Stoumpos, C. C.; Soe, C. M. M.; Tsai, H.; Nie, W.; Blancon, J.-C.; Cao, D. H.; Liu, F.; Traoré, B.; Katan, C.; Even, J.; Mohite, A. D.; Kanatzidis, M. G., High Members of the 2D Ruddlesden-Popper Halide Perovskites: Synthesis, Optical Properties, and Solar Cells of $(CH_3(CH_2)3NH_3)_2(CH_3NH_3)_4Pb_5I_{16}$. *Chem* **2017,** *2*, 427-440.

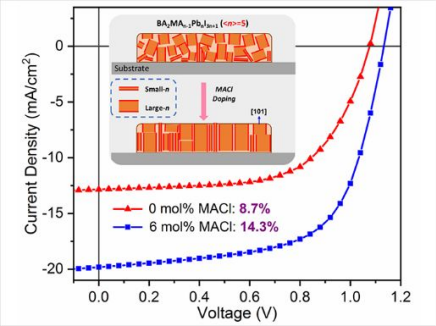

Table of Contents